Materials Chemistry and Physics 203 (2018) 243–248

Contents lists available at ScienceDirect

Materials Chemistry and Physics

journal homepage: www.elsevier.com/locate/matchemphys

Stirrer time effect on optical properties of nanophotonic $LiNbO_3$

Y. Al-Douri [a, b, *], Makram A. Fakhri [c], A. Bouhemadou [d], R. Khenata [e], M. Ameri [f]

[a] Nanotechnology and Catalysis Research Center (NANOCAT), University of Malaya, 50603, Kuala Lumpur, Malaysia
[b] Physics Department, Faculty of Science, University of Sidi-Bel-Abbes, 22000, Algeria
[c] Institute of Nano Electronic Engineering, University Malaysia Perlis, 01000, Kangar, Perlis, Malaysia
[d] Laboratory for Developing New Materials and Their Characterization, Department of Physics, Faculty of Science, University of Setif 1, 19000, Setif, Algeria
[e] Laboratoire de Physique Quantique et de Modélisation Mathématique (LPQ3M), Université de Mascara, 29000, Mascara, Algeria
[f] Physics and Chemistry of Advanced Materials Laboratory, Djillali Liabès University, BP: 89, Sidi Bel-Abbès, 22000, Algeria

HIGHLIGHTS

- Prepare nanophotonic $LiNbO_3$ via feasible method.
- Analyze the optical and structural properties of nanophotonic $LiNbO_3$ under stirrer time.
- Characterize the nanophotonic $LiNbO_3$ under stirrer time.
- Elaborate the refractive index of nanophotonic $LiNbO_3$ for optical applications.

ARTICLE INFO

Article history:
Received 22 October 2015
Received in revised form
7 July 2017
Accepted 7 October 2017
Available online 9 October 2017

Keywords:
Ceramics
Sol-gel growth
Electron microscopy
Optical properties

ABSTRACT

Lithium niobate ($LiNbO_3$) nanostructures are synthesized on n-silicon substrate by spin coating technique with stirrer times; 8 h, 24 h and 48 h. $LiNbO_3$ is characterized and analyzed by Scanning Electron Microscope (SEM), Atomic Force Microscopy (AFM), X-ray diffraction (XRD) and UV-visible and Photoluminescence (PL). The measurements show that as stirrer time increases, the structures start to crystallize to become more regular distribution, which helps to apply in optical waveguides. In addition, the calculated refractive index and optical dielectric constant are in agreement with experimental data.

1. Introduction

Lithium Niobate ($LiNbO_3$) is a very important optical material which is widely used by the photonics industry due to its excellent electro/acousto-optical properties [1,2]. $LiNbO_3$ is an important ferroelectric material because of its excellent piezoelectrical, electrooptical, pyroelectrical and photo-refractive properties [3–6]. It is widely used as polar material for photonic applications [7–9]. In addition, it is employed in nonlinear optics for frequent conversion in telecommunication for electro-optic modulation [10–12]. It is very attractive material for fabrication of optical wave-guide devices [13,14]. This crystal plays an important role as a high quality source material with low optical loss [15] due to their mechanical robustness, good availability, optical homogeneity [16], integrated optics with lasers, modulators [17] and filters on a single $LiNbO_3$ wafer [18]. Thin films of nanophotonic $LiNbO_3$ have been studied in integrated form with unique pyroelectric, piezoelectric and nonlinear optical properties, which would made it an ideal material for fabrication of surface acoustic wave (SAW) [19] and optoelectronic devices [20]. $LiNbO_3$s were prepared using various experimental techniques such as sputtering [21,22], liquid phase epitaxial (LPE) [23], metal organic chemical vapor deposition (MOCVD) [24–26], soft-chemistry [27], hydrothermal methods [28] and pulsed laser deposition (PLD) [29,30].

Bartasyte et al. [31] have deposited $LiNbO_3$ films of high epitaxial quality and with thicknesses of 120–500 nm at 650 °C on C-sapphire by atmospheric pressure metal-organic chemical vapor deposition. They have investigated Li nonstoichiometry, residual stresses, twinning, and thermal expansion of the films as a function

* Corresponding author. Nanotechnology and Catalysis Research Center (NANOCAT), University of Malaya, 50603, Kuala Lumpur, Malaysia.
E-mail address: yaldouri@yahoo.com (Y. Al-Douri).

https://doi.org/10.1016/j.matchemphys.2017.10.024
0254-0584/

of the film thickness by means of Raman spectroscopy and X-ray diffraction, and studied the relaxation of residual stresses, Li_2O loss, inelastic deformation and elastic hysteresis during cycles of heating up to 860 °C and cooling down to room temperature, as well. The residual stresses and thermal expansion of films were highly thickness dependent. It was shown that the $\{01\bar{1}2\}$ twinning contributed to the stress relaxation in the thick $LiNbO_3$ films. While, Lim and Lee [32] have investigated the effects of poly(L-lysine) as a biomolecular additive on the synthesis of $LiNbO_3$. The addition of PLL to a $LiNbO_3$ precursor solution enhanced the aggregation of the produced $LiNbO_3$ nanoparticles. This aggregation was induced by the electrical attraction of PLL with $LiNbO_3$ nanoparticles, and was enhanced with increasing PLL molecular weight. Furthermore, the association of PLL with $LiNbO_3$ nanoparticles was increased by the addition of methanol, which enhanced the miscibility of PLL with the precursor solution working as a co-solvent. The $LiNbO_3$ nanoparticles generated with PLL exhibited piezoelectric properties without post-thermal treatment, suggesting that PLL contributes to the piezoelectricity. Their results are intriguing in terms of the potential for diverse engineering nanomaterials synthesis through a biomolecule that can also improve the physicochemical properties. Furthermore, Nozawa et al. [33] have noticed that the cs-MgO:LN (Li_2O:Nb_2O_5:MgO = 45.3:50.0:4.7) exhibits no segregation of ions during crystal growth. However, a crystallization electromotive force (c-EMF) is observed during growth by the micro-pulling down (μ-PD) method, due to segregation of the cs-MgO:LN ionic species. In this case, the equilibrium partition coefficient, k_0, must be modified to k_{E0} to take into account the effect of an electric field on the partitioning of ionic species. A coefficient of k_{E0} rather than k_0 has a value of non-unity and therefore can lead to generation of a c-EMF.

This paper reports the $LiNbO_3$ nanostructures by utilizing spin coating technique. XRD, SEM, AFM, PL and UV-visible studied the phase evolution with the stirrer time. The refractive index is the main study for optical waveguides from $LiNbO_3$ nanostructures because of refraction coefficients between the base and deposited films will ensure access to total internal reflection for giving better result of optical waveguide. Optical waveguides of high index contrast enable small cross section dimensions and small bending radii of curved waveguides, a prerequisite for high density integrated optics. The paper is organized as the followings; Section 2 details the experimental procedure. The results and discussion are elaborated in section 3. Finally, conclusion is summarised in section 4.

2. Experimental process

The preparation procedure for $LiNbO_3$ nanostructures is using Nb_2O_5 (ultra-purity, 99.99%), and cetric acid (C.A.) without further purification. The solution is prepared by mixing Li_2CO_3, Nb_2O_5, citric acid and Ethylene Glycol. The molar ratio between Li_2Co_3 and Nb_2O_5 was 1:1 in order to maximize the formation of $LiNbO_3$ stoichiometry phase as follow (Li_2Co_3 = 0.925, 1.85, 2.775 and 3.7 gm, Nb_2O_5 = 3.325, 6.650, 9.975 and 13.30 gm, CA = 2.625, 5.25, 7.875 and 10.5 gm and EG = 20 mm^3). Firstly, the $LiCo_3$, Nb_2O_5 and citric acid were dissolved in Ethylene Glycol with heating and stirring at 90 °C for 8 h, 24 h and 48 h, then mixed altogether with continue heating and stirring at 90 °C for 8 h, 24 h and 48 h. To obtain homogeneous and crack-free films of $LiNbO_3$, the precursor was deposited by spin coating technique on n-silicon substrates at 3000 rpm for 30 s, 0.5 M/L and annealed at 500 °C. Seven layers were prepared, the film was dried at 120 °C for 5 min and calcined at 250 °C for 30 min in static air and oxygen atmosphere to remove the organics, then it was annealing at 500 °C. The structural evolution of the as-prepared thin films was examined using high-resolution X-ray diffraction (HR-XRD), (X'Pert Pro MRD PW3040 system diffractometer, PANalytical Company, Netherlands) system equipped with Cu-K α-radiation of wavelength λ = 0.15418 nm at 40 kV and 30 mA. The thickness of the annealed samples was studied using Scanning Optical Reflectometer model (Filmetrics F20, China). The Scanning Electron Microscopy (JOEL JSM-6460LV, Oxford instruments Analytical Ltd., Japan) was used to investigate the surface morphology of $LiNbO_3$, and Atmoic Force Microscopy (AFM) (SPM-9600, Scanning Probe Microscope, Shimadzu, Japan) was utilized for investigating the roughness of $LiNbO_3$. The optical properties were investigated using the double-beam Ultr-Violet (UV-vis) spectrophotometer (Shimadzu UV-Vis 1800, Japan) and photoluminescence (PL) spectroscopy system (Jobin Yvon model HR 800 UV system, Kyoto, Japan) at room temperature using He-Cd laser (λ = 352 nm).

3. Results and discussion

3.1. Structural properties

The crystalline structure of $LiNbO_3$ nanostructures is found to have hexagonal structure as shown in Fig. 1. It is observed that the peaks at 2θ = 23.634, 32.637, 34.674, 48.355, 53.106, and 55.879 correspond to (012), (104), (110), (024), (116) and (122) planes. All the mentioned peaks are exactly matched with the crystalline structure of $LiNbO_3$ nanostructures that corresponding to the standard (ICDD PDF2008, 00-029-0537). Therefore, the crystalline structure will be crystalline and more purity for $LiNbO_3$ with increasing stirrer time due to increasing the peak intensity. The measured structural properties of $LiNbO_3$ nanostructures are listed in Table 1. Crystallite size (D) was calculated using Scherrer's formula [34].

$$D = K\lambda/\beta\cos\theta \quad (1)$$

where K is a constant taken to be 0.94, λ is the wavelength of X-ray used (λ = 1.54 Å), β is the full width at half maximum of XRD pattern and θ is Bragg's angle, around 26.41°.

In addition, the dislocation density (δ) and strain (ε) of $LiNbO_3$ nanostructures were determined using the following relations [35].

$$\delta = 1/D^2 \quad (2)$$

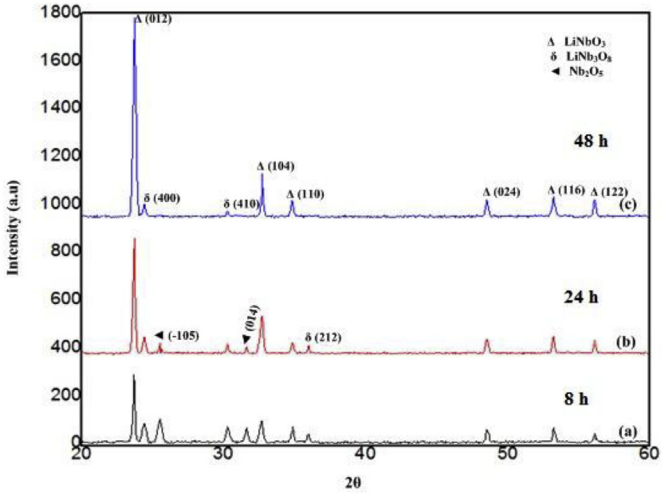

Fig. 1. XRD patterns of $LiNbO_3$ nanostructures at different stirrer times (a) 8 h, (b) 24 h and (c) 48 h.

Table 1
Structural parameters of $LiNbO_3$ nanostructures at different stirrer times.

Stirrer time (h)	Orientation *hkl*	Peak (θ)	Particle size (nm)	Dislocation density (δ) (10^{14}) (lines/m^2)	Strain (10^{-3})	d_{hkl} (Å)	Lattice constants (Å)	Roughness (nm)
8	012	23.7388	92.63718	0.000117	0.835339	3.74508	a = 5.1566 c = 13.85	5.5
	104	33.0318	47.27894	0.000447	0.839386	2.709617	a = 5.1566 c = 13.85	
	110	35.2249	71.33627	0.000197	0.488195	2.545778	a = 5.1566 c = 13.85	
	024	47.5173	59.43061	0.000283	0.31739	1.911945	a = 5.1566 c = 13.85	
	116	54.6075	51.0116	0.000384	0.276939	1.679269	a = 5.1566 c = 13.85	
	122	58.3125	38.92867	0.00066	0.316165	1.581086	a = 5.1566 c = 13.85	
24	012	23.7137	55.57975	0.000324	0.83716	3.748987	a = 5.1566 c = 13.85	14.1
	104	33.0375	56.73556	0.000311	0.41954	2.709163	a = 5.1566 c = 13.85	
	110	35.1878	34.23789	0.000853	0.611616	2.548377	a = 5.1566 c = 13.85	
	024	47.4937	44.56892	0.000503	0.254196	1.91284	a = 5.1566 c = 13.85	
	116	54.3849	15.28818	0.004278	0.55919	1.685616	a = 5.1566 c = 13.85	
	122	56.5445	23.16062	0.001864	0.34019	1.626253	a = 5.1566 c = 13.85	
48	012	23.6909	18.52581	0.002914	0.838819	3.752543	a = 5.1566 5.1561[a] 5.49340[b] c = 13.85 13.8669[a]	20.9
	104	33.0227	14.18335	0.004971	0.559917	2.710343	a = 5.1566 c = 13.85	
	110	35.1816	19.00238	0.002769	0.375023	2.573661	a = 5.1566 c = 13.85	
	024	48.7281	4.975972	0.040387	0.719699	1.86723	a = 5.1566 c = 13.85	
	116	54.3477	4.367322	0.052429	0.653432	1.686682	a = 5.1566 c = 13.85	
	122	58.2137	7.705445	0.016842	0.346083	1.637142	a = 5.1566 c = 13.85	

[a] Ref. [55] exp.
[b] Ref. [56] exp.

$$\varepsilon = \beta/4\tan\theta. \quad (3)$$

The interplanar distance (d) is calculated for all set of $LiNbO_3$ nanostructures using Bragg's formula [35].

$$d = h\lambda/2\sin\theta. \quad (4)$$

where h is Miller index. The lattice parameters a and c were calculated by Ref. [36];

$$\frac{1}{d^2} = \frac{4}{3}\left(\frac{h^2 + hk + k^2}{a^2}\right) + \frac{l^2}{c^2} \quad (5)$$

All the reflection peaks could be indexed to the hexagonal structure with lattice constants $a = b = 5.145$, $c = 13.858$, which were very close to the reported data [37]. The thin film was a polycrystalline structure after annealing at 500 °C for 2 h in static air, two phases of lithium niobate could be recognized, Δ and δ phases. This phase (δ) is originated from an interface reaction between the Oxygen and $LiNbO_3$ then could be detected by XRD due to its high crystallization temperature and will be decreased as the stirrer time increases leading to possibility for total interaction between the chemicals to improve the purity of the final solvent mixture. It is found at peaks $2\theta = 24.407$ and 30.262 correspond to (400) and (410) planes at high stirrer time, and at peak 35.981 corresponds to (212) plane at low stirrer time. This is attributed to annealing effect in static air, oxygen atmosphere and total interaction between the chemicals. There is no impurities like Nb_2O_5, were detected in high stirrer time because of increased hours of mixing, but in low stirrer time we find Nb_2O_5 at peaks $2\theta = 24.433$ and 31.623 correspond to (−105) and (014) planes as raw material. Fig. 1 shows nanophotonic $LiNbO_3$ with different peaks, including main diffraction for (012) plane, at different stirrer times. As stirrer times increase, the mean particle size decreases because the stirrer time leads to complete solving of chemical interaction as explained in Table 1. The purity of nanophotonic $LiNbO_3$ and increasing of time period of solubility process affect on crystallization, therefore we get a solution free of impurities and high crystallization as shown in Fig. 1c, comparing to Fig. 1(a and b).

3.2. Optical properties

The optical reflectance of $LiNbO_3$ was studied in the wavelength range 300–800 nm at room temperature. Fig. 2a shows the variation of reflectance of surface with wavelength of $LiNbO_3$ nanostructure. The optical band gaps were determined with the help of reflection spectra [38,39]. Almost all the II–VI compounds are direct band gap semiconductors. According to Tauc relation [39,40], the absorption coefficient for direct band gap material is given by;

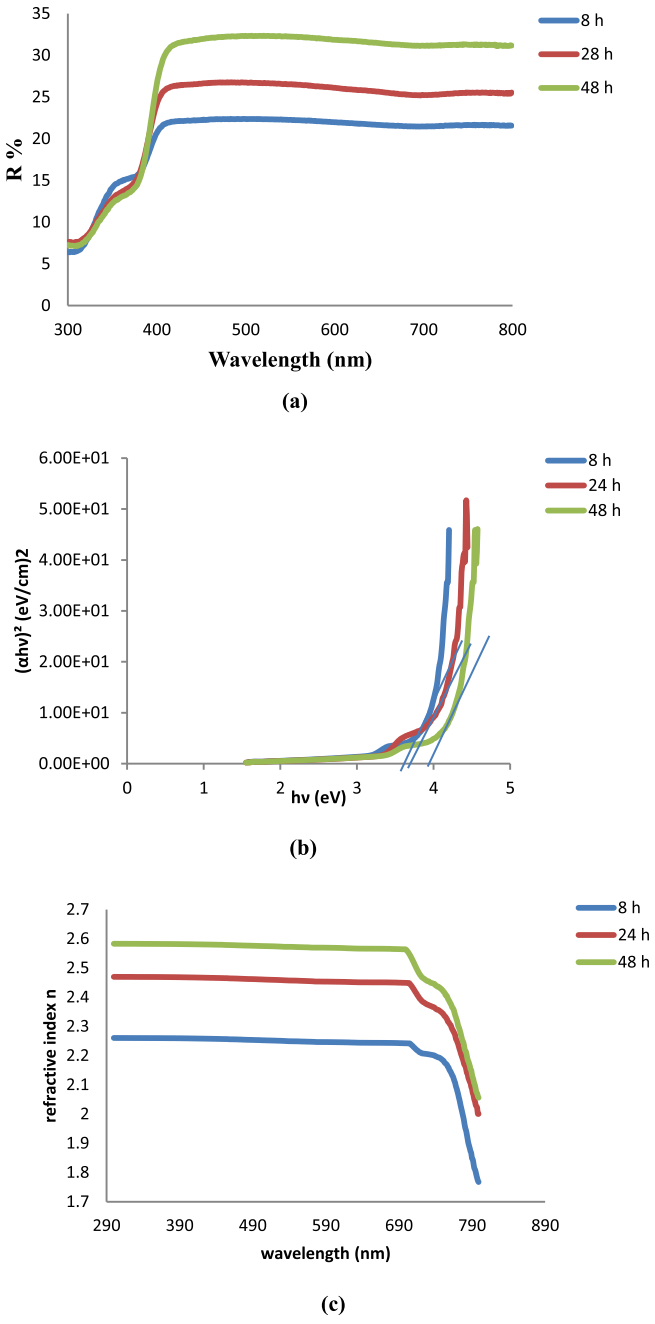

Fig. 2. (a) Reflection spectra, (b) Energy band gap and (c) Refractive index of $LiNbO_3$ nanostructures at different stirrer times (a) 8 h, (b) 24 h and (c) 48 h.

$$\alpha h\upsilon = A(h\upsilon - Eg)^n \tag{6}$$

where $h\upsilon$ is photon energy, A is constant, E_g is the band gap and n is equal to ½ for direct band gap material. To measure energy band gap from reflection spectra, a graph between $(\alpha h\upsilon)^2$ vs. $h\upsilon$ is plotted. Absorption coefficient α is proportional to $\ln[(R_{max}\text{-}R_{min})/(R\text{-}R_{min})]$ [41] where reflectance falls from max R to min R due to absorption by the material and R is the reflectance for any intermediate energy photons. The reflectance percentage decreases as stirrer time increases as given in Table 2. The energy band gap (E_g) is found by plotting $(\alpha h\nu)^2$ vs. $h\nu$ as shown in Fig. 2b [41,42]. The extrapolation of straight line to $(\alpha h\upsilon)^2 = 0$ gives the value of direct band gap. From this graph, the value of energy band gap comes out to be 3.97 eV (Table 2).

The refractive index (n) was determined from a transmittance spectrum as a function of the wavelength in the range 300–700 nm. There is a decreasing in the refractive index may be attributed to invisible range; it was estimated 2.26–2.58 at 330 nm as shown in Fig. 2c and given in Table 2. The refractive index changes slightly and steadily after 330 nm–700 nm as shown in Fig. 2c. We can notice from that, the refractive index increases as stirrer time increases. This behavior may be attributed to increasing of thickness due to multilayer deposition (Table 2). The highest values of refractive index are suitable for optical waveguide. Intuitive, increasing stirrer time leads to increase thickness of synthesized $LiNbO_3$ nanostructures that correlate directly with refractive index as confirmed in Fig. 2c.

The photoluminescence (PL) spectra of $LiNbO_3$ nanostructures are grown on n-Si substrate at 25 °C as shown in Fig. 3, where emissions are appeared in 313 (3.961 eV) within 48 h, 325 (3.815 eV) within 24 h and 336 (3.691 eV) within 8 h. The peak at 313 nm is more intense. A central factor of this discussion is the nature of the characterized samples. It must be pointed out that the $LiNbO_3$ nanostructures used to study PL behavior are usually synthesized with distinct method. Furthermore, the relative peak intensities of each peak depend also on the corresponding radiative recombination efficiency. Thus, PL spectra of $LiNbO_3$ nanostructures demonstrate that the produced material has enough quality to be used in the research of semiconductor devices and optoelectronics. This trend can be understood that surface-to-volume ratio becomes smaller with increasing grain size, and the larger grains have smaller nonradiative relaxation rates over the surface states resulting in the enhancement of PL intensity. On the other hand, it is noted clearly a blue shift in PL and UV-vis, where the band gap values increase from 3.6 to 3.9 eV with increasing of stirrer times, that can be attributed to improvement of nano-photonic $LiNbO_3$ crystals [39].

The refractive index n is a significant physical parameter in microscopic atomic interactions. Theoretically, the refractive index is related to the density and the local polarizability of these entities [43]. Many simple relationships between refractive index n and the energy gap E_g have been attempted [44–51]. Here, various relationships between n and E_g have been reviewed in order to validate the current work. As suggested by Ravindra et al. [44], the band gap and the high frequency refractive index, presented a linear relationship:

$$n = \alpha + \beta E_g, \tag{7}$$

where $\alpha = 4.048$ and $\beta = -0.62$ eV^{-1}

Inspired by simple physics of light refraction and dispersion, Herve and Vandamme [45] have proposed an empirical relation as:

$$n = \sqrt{1 + \left(\frac{A}{E_g + B}\right)^2} \tag{8}$$

where $A = 13.6$ eV and $B = 3.4$ eV.

Ghosh et al. [46] had taken a different approach by considering the band structural and quantum-dielectric formulations of Penn [52] and Van Vechten [53]. Introducing, A (contribution from the valence electrons) and B (constant additive to the lowest band gap E_g), the expression was written as:

$$n^2 - 1 = A / (E_g + B)^2, \tag{9}$$

where $A = 25E_g + 212$, $B = 0.21E_g + 4.25$ and $(E_g + B)$ refers to an appropriate average energy gap of the material.

Table 2
The energy band gaps and refractive index correspond to grain size of $LiNbO_3$ nanostructures at different stirrer times.

Stirrer time (h)	E_g (UV-vis) (eV)	E_g (PL) (eV)	E_g (eV) exp [57].	*n (measured)*	*n* exp. [58]	*n (calculated)*	ε_∞	R (%)
8	3.61	3.691	2.66–4.22	2.26	2.42	1.79[a] 2.173[b] 2.246[c] 2.77[a] 2.171[b] 2.242[c]	3.20[a] 4.72[b] 5.046[c] 7.67[a] 4.71[b] 5.027[c]	33.23
24	3.72	3.815		2.48		1.78[a] 2.172[b] 2.245[c] 2.76[a] 2.170[b] 2.241[c]	3.16[a] 4.715[b] 5.041[c] 7.61[a] 4.706[b] 5.02[c]	26.5
48	3.97	3.961		2.58		1.77[a] 2.171[b] 2.244[c] 2.75[a] 2.169[b] 2.240[c]	3.13[a] 4.711[b] 5.03[c] 7.56[a] 4.702[b] 5.01[c]	21.65

[a] Ref. [44].
[b] Ref. [45].
[c] Ref. [46].

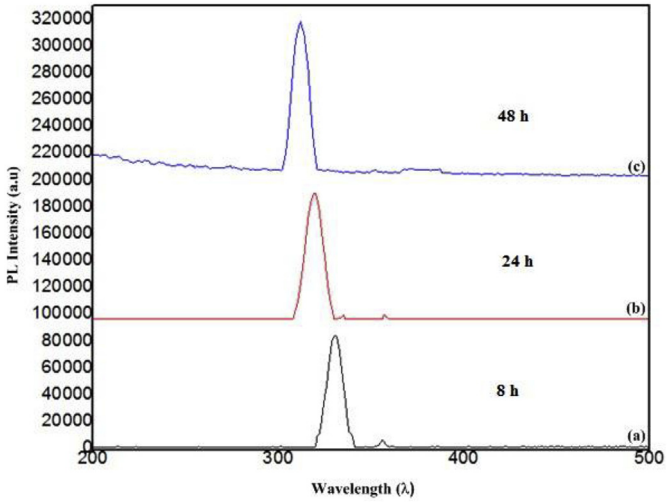

Fig. 3. PL spectra of $LiNbO_3$ at different stirrer times (a) 8 h, (b) 24 h and (c) 48 h.

Thus, these three models for variation of *n* with energy gap have been tried. In addition, the calculated values of the optical dielectric constant (ε_∞) were obtained using the relation $\varepsilon_\infty = n^2$ [54]. The calculated refractive index and optical dielectric constant are given in Table 2. This is showing that the Ghosh et al. model is an appropriate model for solar cells applications due to its agreement with experimental refractive index value [58].

4. Conclusions

The $LiNbO_3$ nanostructures have been chemically prepared by spin-coating technique. Based on XRD results, the $LiNbO_3$ nanostructures have polycrystalline in nature. The intensity is 900 a.u corresponds to (012) at $2\theta = 23.634$. As expected, the structure is more crystalline as the time of stirrer increases. In addition, SEM explains the prepared $LiNbO_3$ to be embodied as stirrer time increases. AFM shows diameter of gain size from 18 to 92 nm, and roughness ranging between 5 and 20 nm. Optical properties give values of reflection that is about 21–33% and the measured energy band gaps are between 3.61 and 3.97 eV. We found an approximated matching between the energy gaps values calculated using UV-vis and PL. The highest value of *n* is an appropriate for optical waveguide. Refractive index determined from specific empirical models revealed that the highest value and Ghosh et al. model is more appropriate for optical waveguide.

References

[1] S. Grilli, Ferroelectric Domain Engineering and Characterization for Photonic Applications, Doctoral Thesis, Department of Physics, Royal Institute of Technology, Stockholm, Sweden, 2006.
[2] E. Marenna, C. Aruta, E. Fanelli, M. Barra, P. Pernice, A. Aronne, Sol–gel synthesis of nanocomposite materials based on lithium niobate nanocrystals dispersed in a silica glass matrix, J. Solid State Chem. 182 (2009) 1229–1234.
[3] P. Kumar, S.M. Babu, S. Perero, R.L. Sai, I. Bhaumik, S.G. Morthy, A.K. Karnal, X-ray photoelectron spectroscopy, high-resolution X-ray diffraction and refractive index analyses of Ti-doped lithium niobate (Ti:$LiNbO_3$) nonlinear optical single crystal, Pramana J. Phys. 75 (2010) 1035–1040.
[4] G.W. Burr, S. Diziain, M.P. Bernal, Theoretical study of lithium niobate slab waveguides for integrated optics applications, Opt. Mater. 31 (2009) 1492–1497.
[5] F. Meriche, A. Boudrioua, R. Kremer, E. Dogheche, E. Neiss-Clauss, R. Mouras, A. Fischer, M.-R. Beghoul, E. Fogarassy, N. Boutaoui, Fabrication and investigation of 1D and 2D structures in $LiNbO_3$ thin films by pulsed laser ablation, Opt. Mater. 32 (2010) 1427–1434.
[6] M. Aufray, S. Menuel, Y. Fort, J. Eschbach, D. Rouxel, B. Vincent, New synthesis of nanosized niobium oxides and lithium niobate particles and their characterization by XPS analysis, J. Nanosci. Nanotechnol. 9 (2009) 4780–4785.
[7] L. Cao, A. Aboketaf, Z. Wang, S. Preble, Hybrid amorphous silicon (a-Si:H)–LiNbO3 electro-optic modulator, Opt. Commun. 330 (2014) 40–44.
[8] H. Chen, T. Lv, A. Zheng, Y. Han, Discrete diffraction based on electro-optic effect in periodically poled lithium niobate, Opt. Commun. 294 (2013) 202–207.
[9] H. Hu, R. Ricken, W. Sohler, Lithium niobate photonic wires, Opt. Express 17 (2009) 24261–24268.
[10] D. Sun, Z. Liu, Y. Huang, S. Ho, D.J. Towner, B.W. Wessels, Performance simulation for ferroelectric thin-film based waveguide electro-optic modulators, Opt. Commun. 255 (2005) 319–330.
[11] G. Poberaj, M. Koechlin, F. Sulser, A. Guarino, J. Hajfler, P. Günter, Ion-sliced lithium niobate thin films for active photonic devices, Opt. Mater. 31 (2009) 1054–1058.
[12] T. Zhang, B. Wang, Y. Zhao, S. Fang, D. Ma, Y. Xu, Optical homogeneity and second harmonic generation in Li-rich Mg-doped LiNbO3 crystals, Mater. Chem. Phys. 88 (2004) 97–101.
[13] L. Chen, Q. Xu, M.G. Wood, R.M. Reano, Hybrid silicon and lithium niobate electro-optical ring modulator, Optica 1 (2014) 112–118.
[14] W. Kim, S.-W. Kwon, W. Jeong, G. Son, K. Lee, W. Choi, W. Yang, H. Lee, H. Lee, Integrated optical modulator for signal upconversion over radio-on-fiber link, Opt. Express 17 (2009) 2638–2645.
[15] R. Lin, Y. Gao, Factors that influence the modulation instability in self-defocusing photorefractive crystal, Opt. Commun. 285 (2012) 2724–2728.
[16] J. Guo, J. Zhu, W. Zhou, X. Huang, A plasmonic electro-optical variable optical attenuator based on side-coupled metal–dielectric–metal structure, Opt. Commun. 294 (2013) 405–408.
[17] H.K. Lam, J.Y. Dai, H.L.W. Chan, Orientation controllable deposition of LiNbO3 films on sapphire and diamond substrates for surface acoustic wave device application, J. Cryst. Growth 268 (2004) 144–148.
[18] R. Grange, J.-W. Choi, C. Hsieh, Y. Pu, A. Magrez, R. Smajda, L. Forró, D. Psaltis, Lithium niobate nanowires synthesis, optical properties, and manipulation, Appl. Phys. Lett. 95 (2009), 143105–1-143107.
[19] Y. Tan, F. Chen, M. Stepić, V. Shandarov, D. Kip, Reconfigurable optical channel waveguides in lithium niobate crystals produced by combination of low-dose O3+ ion implantation and selective white light illumination, Opt. Express 16 (2008) 10465–10470.
[20] Z. Zhou, B. Wang, Sh Lin, Y. Li, K. Wang, Investigation of optical photorefractive properties of Zr:Fe:LiNbO3 crystals, Opt. Laser Technol. 44 (2012) 337–340.
[21] L.H. Wang, D.R. Yuan, X.L. Duan, X.Q. Wang, F.P. Yu, Synthesis and characterization of fine lithium niobate powders by sol- gel method, Cryst. Res. Technol. 42 (2007) 321–324.
[22] Y. Lu, P. Dekker, Growth and characterization of lithium niobate planar waveguides by liquid phase epitaxy, J. Cryst. Growth 311 (2009) 1441–1445.
[23] Y. Akiyama, K. Shitanaka, H. Murakami, Y. Shin, M. Yoshida, N. Imaishi, Epitaxial growth of lithium niobate film using metalorganic chemical vapor deposition, Thin Solid Films 515 (2007) 4975–4979.
[24] R. Ageba, Y. Kadota, T. Maeda, N. Takiguchi, T. Morita, Ultrasonically-assisted

hydrothermal method for ferroelectric material synthesis, J. Korean Phys. Soc. 57 (2010) 918–923.
[25] Y. Kang, S. Jeong, S. Lee, J. Hwang, J. Kim, C. Cho, Hetero-epitaxial growth of $LiNbO_3$ thin film on GaN/Al2O3 by pulsed laser deposition, J. Korean Phys. Soc. 49 (2006) S625–S628.
[26] J. Son, S.S. Orlov, B. Phillips, L. Hesselink, Pulsed laser deposition of single phase LiNbO3 thin film waveguides, J. Electroceramics 17 (2006) 591–595.
[27] M. Nyman, T.M. Anderson, P.P. Provencio, Comparison of aqueous and non-aqueous soft-chemical syntheses of lithium niobate and lithium tantalate powders, Cryst. Growth Des. 9 (2009) 1036–1040.
[28] B.K. Yun, Y.K. Park, M. Lee, N. Lee, W. Jo, S. Lee, J. Hoon Jung, Lead-free $LiNbO_3$ nanowire-based nanocomposite for piezoelectric power generation, Nano-scale Res. Lett. 9 (2014) 4–10.
[29] X. Wang, Z. Ye, G. Wu, L. Cao, B. Zhao, Growth of textured $LiNbO_3$ thin film on Si (111) substrate by pulsed laser deposition, Mater. Lett. 59 (2005) 2994–2997.
[30] X. Wang, Y. Liang, S. Tian, W. Man, J. Jia, Oxygen pressure dependent growth of pulsed laser deposited $LiNbO_3$ films on diamond for surface acoustic wave device application, J. Cryst. Growth 375 (2013) 73–77.
[31] A. Bartasyte, V. Plausinaitiene, A. Abrutis, S. Stanionyte, S. Margueron, V. Kubilius, P. Boulet, S. Huband, P.A. Thomas, Thickness dependent stresses and thermal expansion of epitaxial LiNbO3 thin films on C-sapphire, Materials Chemistry and Physics (2015) 622–631, 149–150.
[32] Youngjoon Lim, Sang-Yup Lee, Preparation of LiNbO3 nanoparticles using poly(l-lysine) as a biomolecular additive, Mater. Chem. Phys. 144 (2014) 92–97.
[33] Jun Nozawa, Shintaro Iida, Chihiro Koyama, Kensaku Maeda, Kozo Fujiwara, Haruhiko Koizumi, Satoshi Uda, Partitioning of ionic species during growth of impurity-doped lithium niobate by electric current injection, J. Cryst. Growth 406 (2014) 78–84.
[34] Y. Al-Douri, Q. Khasawneh, S. Kiwan, U. Hashim, S.B. Abd Hamid, A.H. Reshak, A. Bouhemadou, M. Ameri, R. Khenata, Structural and optical insights to enhance solar cell performance of CdS nanostructures, Energy Convers. Manag. 82 (2014) 238–243.
[35] M.A. Fakhri, Y. Al-Douri, U. Hashim, E.T. Salim, Optical investigations of photonics lithium niobate, Sol. Energy 120 (2015) 381–388.
[36] A.S. Ibraheam, Y. Al-Douri, U. Hashim, M.R. Ghezzar, A. Addou, W.K. Ahmed, Cadmium effect on optical properties of $Cu_2Zn_{1-x}Cd_xSnS_4$ quinternary alloys nanostructures, Sol. Energy 114 (2015) 39–50.
[37] A.Z. Simoes, M.A. Zaghetea, B.D. Stojanovic, C.S. Riccardi, A. Ries, A.H. Gonzalez, J.A. Varela, $LiNbO_3$ thin films prepared through polymeric precursor method, Mater. Lett. 57 (2003) 2333–2339.
[38] V. Kumar, S.K. Sharma, T.P. Sharma, V. Singh, Band gap determination in thick films from reflectance measurements, Opt. Mater. 12 (1999) 115–119.
[39] Makram A. Fakhri, Y. Al-Douri, U. Hashim, Evan T. Salim, Deo Prakash, K.D. Verma, Optical investigation of nanophotonic lithium niobate-based optical waveguide, Appl. Phys. B 121 (2015) 107–116.
[40] E.T. Salim, Y. Al-Douri, M.S. Al Wazny, M.A. Fakhri, Optical properties of Cauliflower-like Bi2O3 nanostructures by reactive pulsed laser deposition (PLD) technique, Sol. Energy 107 (2014) 523–529.
[41] A.Z. Simões, A.H.M. González, A.A. Cavalheiro, M.A. Zaghete, B.D. Stojanovic, J.A. Varela, Effect of magnesium on structure and properties of $LiNbO_3$ prepared from polymeric precursors, Ceram. Int. 28 (2002) 265–270.
[42] I.-K. Jeong, Correlated thermal motion in ferroelectric $LiNbO_3$ studied using neutron total scattering and a rietveld analysis, J. Korean Phys. Soc. 59 (2011) 2756–2759.
[43] N.M. Balzaretti, J.A.H. da Jornad, Pressure dependence of the refractive index of diamond, cubic silicon carbide and cubic boron nitride, Solid State Commun. 99 (1996) 943–948.
[44] N.M. Ravindra, S. Auluck, V.K. Srivastava, On the penn gap in semiconductors, Phys. Stat. Sol.(B) 93 (1979) k155–K160.
[45] P.J.L. Herve, L.K.J. Vandamme, Empirical temperature dependence of the refractive index of semiconductors, J. Appl. Phys. 77 (1995) 5476–5477.
[46] D.K. Ghosh, L.K. Samanta, G.C. Bhar, A simple model for evaluation of refractive indices of some binary and ternary mixed crystals, Infrared Phys. 24 (1984) 43–47.
[47] Y. Al-Douri, H. Khachai, R. Khenata, Chalcogenides-based quantum dots: optical investigation using first-principles calculations, Mater. Sci. Semicond. Process. 39 (2015) 276–282.
[48] Y. Al-Douri, U. Hashim, R. Khenata, A.H. Reshak, M. Ameri, A. Bouhemadou, A. Rahim Ruslinda, M.K. Md Arshad, Ab initio method of optical investigations of $CdS_{1-x}Te_x$ alloys under quantum dots diameter effect, Sol. Energy 115 (2015) 33–39.
[49] Y. Al-Douri, Electronic and optical properties of $Zn_xCd_{1-x}Se$, Mater. Chem. Phys. 82 (2003) 49–54.
[50] Y. Al-Douri, Y.P. Feng, A.C.H. Huan, Optical investigations using ultra-soft pseudopotential calculations of $Si_{0.5}Ge_{0.5}$ alloy, Solid State Commun. 148 (2008) 521–524.
[51] Y. Al-Douri, A.H. Reshak, H. Baaziz, Z. Charifi, R. Khenata, S. Ahmad, U. Hashim, An ab initio study of the electronic structure and optical properties of $CdS_{1-x}Te_x$ alloys, Sol. Energy 84 (2010) 1979–1984.
[52] D.R. Penn, Wave-number-dependent dielectric function of semiconductors, Phys. Rev. 128 (1962) 2093–2100.
[53] J.A. Van Vechten, Quantum dielectric theory of electronegativity in covalent systems. I. Electronic dielectric constant, Phys. Rev. 182 (1969) 891–905.
[54] G.A. Samara, Temperature and pressure dependences of the dielectric constants of semiconductors, Phys. Rev. B 27 (1983) 3494–3505.
[55] N.S.L.S. Vasconcelos, J.S. Vasconcelos, V. Bouquet, S.M. Zanetti, E.R. Leite, E. Longo, L.E.B. Soledade, F.M. Pontes, M. Guilloux-Viry, A. Perrin, M.I. Bernardi, J.A. Varela, Epitaxial growth of LiNbO thin films in a microwave oven, Thin Solid Films 436 (2003) 213–219.
[56] D.E. Zelmon, D.L. Small, Infrared corrected Sellmeier coefficients for congruently grown lithium niobate and 5 mol. % magnesium oxide–doped lithium niobate, J. Opt. Soc. Am. B 14 (1997) 3319–3323.
[57] Y. Akaltun, M.A. Yıldırım, A. Ateş, M. Yıldırım, The relationship between refractive index-energy gap and the film thickness effect on the characteristic parameters of CdSe thin films, Opt. Commun. 284 (2011) 2307–2311.
[58] M.A. Yıldırım, A. Ates, Influence of films thickness and structure on the photoresponse of ZnO films, Opt. Commun. 283 (2010) 1370–1377.